

1 **Assessment of variability of TEC and improvement of**  
2 **performance of the IRI model over Ethiopia during**  
3 **the high solar activity phase**

4 Yekoye Asmare Tariku

5 Ethiopian Space Science and Technology Institute, Addis Ababa, Ethiopia

6  
7 \* Corresponding author. Tel. +251912799754

8 *Email\_address:yekoye2002@gmail.com (Yekoye Asmare)*

9 **Abstract**

10 This paper discusses the monthly and seasonal variation of the total electron content (TEC) and  
11 the improvement of performance of the IRI model in estimating TEC over Ethiopia during the  
12 solar maximum (2013-2016) phase employing GPS TEC data inferred from the GPS receivers  
13 installed at different regions of Ethiopia. **The results reveal that, in the year 2013-2016, the**  
14 **highest peak measured seasonal diurnal VTEC value is observed in the March equinox in**  
15 **2015 over Arba Minch station.** Moreover, both the arithmetic mean measured and modeled  
16 VTEC values, generally, show maximum and minimum values in the equinoctial and June  
17 solstice months, respectively in 2014-2015. **However, in 2013, the minimum and maximum**  
18 **arithmetic mean measured values are observed in the March equinox and December**  
19 **solstice, respectively.** The results also show that, even though overestimation of the modeled  
20 VTEC has been observed on most of the hours, all versions of the model are generally good to  
21 estimate both the monthly and seasonal diurnal hourly VTEC values, especially in the early

22 morning hours (00:00-03:00 UT or 03:00-06:00 LT). **It has also been shown that the IRI 2007**  
23 **and IRI 2012 versions are generally better when the solar activity decreases; while IRI 2016**  
24 **is better when the solar activity increases to capture the GPS VTEC values. In addition, the**  
25 **IRI 2012 version with IRI2001 option for the topside electron density shows the highest**  
26 **overestimation of the VTEC as compared to the other options.** All versions of the model do  
27 not also able to capture the effects resulting from storm.

28 **Key words:** GPS-VTEC; IRI- VTEC; GPS signal, solar maximum

29

## 30 **1. Introduction**

31 The energy transferred from the sun causes atoms and molecules existing in the  
32 atmosphere to undergo chemical reactions and become ionized (Kelley, 2009). This ionized and  
33 conductive region of Earth's atmosphere, extending from about 50 to 1000 km and possessing  
34 free electrons and positive ions generally in equal numbers in a medium that is electrically  
35 neutral, is termed as ionospher. The existence of these ions (plasma) in the ionosphere results in  
36 the possibility of radio communications over large distance by making use of one or more  
37 ionospheric reflections (Hunsucker and Hargreaves, 2003).

38 On the other hand, the ionosphere affects the electromagnetic waves that pass through it  
39 by inducing additional transmission time delay (Gao and Liu, 2002). Because of its dispersive  
40 character, electromagnetic signals (such as GPS signals) experience time delay (modulated  
41 codes) and advance (carrier phase) as they propagate through the ionosphere. This delay is  
42 directly proportional to the integral number of electrons in a unit cross-sectional area (usually  
43 referred to as total electron content, TEC) along the signal path extending from the satellite to the  
44 receiver on the ground, and inversely proportional to the square of the frequency of propagation

45 (Hofmann-Wellenhof et al., 1992; Misra and Enge, 2006). The dispersive ionosphere introduces  
46 a time delay in the 1.57542 GHz (L1) and 1.22760 GHz (L2) simultaneous transmissions from  
47 GPS satellites orbiting at 20,200 km (Hansen et al., 2000). The relative ionospheric delay of the  
48 two signals is proportional to the TEC. Time delay measurements of L1 and L2 frequencies can,  
49 therefore, be converted to TEC along the ray path from the receiver to the satellite (Lanyi and  
50 Roth, 1988). The GPS signals traverses the ionosphere carrying signatures of the dynamic  
51 medium and thus offers opportunities for ionospheric research. As a result, global and regional  
52 maps of ionospheric TEC can be produced using data from the worldwide network of the  
53 International GPS Service (Lanyi and Roth, 1988). The availability of TEC measurements is also  
54 important to the development of ionospheric models such as the International Reference  
55 Ionosphere, IRI (Bilitza, 2001). The International Reference Ionosphere (IRI) is an international  
56 project sponsored by the Committee on Space Research (COSPAR) and the International Union  
57 on Radio Science (URSI).

58 Using the GPS satellites and the IRI model, there have been so far several researches  
59 conducted globally in connection with the TEC variability and performance of the model over  
60 equatorial and low latitude regions, **especially using IRI 2007 and IRI 2012 versions (e.g.**  
61 **Ezquer et al., 2014; Luhr and Xiong, 2010; Nigussie et al., 2013; Sethi et al., 2011; Olwendo**  
62 **et al., 2012a; Olwendo et al., 2012b).** Nigussie et al., 2013, for instance, reported that IRI  
63 **2007 model overestimates the VTEC values over the East African equatorial regions. Using**  
64 **IRI 2007, Sethi et al., 2011, also showed that using IRI 2007 model with IRI 2001 option for**  
65 **the topside electron density highly overestimates the VTEC in all seasons and times over**  
66 **low and equatorial Indian regions.** Olwendo et al. (2012a) also noted that seasonal average  
67 IRI 2007 TEC values were higher than the GPS-TEC data for the period of 2009-2011 over

68 different regions in Kenya. In addition, Olwendo et al. (2012b) reported that the IRI 2007 TEC is  
69 too high for all seasons except for the March equinox (where there seems to be good agreement  
70 between observation and model) during the lowest solar activity phase (2009-2010). Ezquer et al.  
71 (2014), using IRI 2012, noted that IRI 2012 predictions show significant deviations from  
72 experimental values during the period of 2008-2009 for a station placed at the southern crest of  
73 the equatorial anomaly in the American region. The report of Kumar (2016) on the validation of  
74 the IRI 2012 models for the global equatorial region also showed that the IRI 2012 model  
75 generally overestimated the observed VTEC over equatorial regions during the solar minimum  
76 year (2009) and solar maximum (2012) phases. Asmare et al. (2014) and Tariku, 2015a and  
77 Tariku, 2015b also attempted to see patterns in both the measured and modeled VTEC variations  
78 during the low and high solar activity phases employing different GPS stations and IRI 2012  
79 model at various regions of Ethiopia. Asmare et al. (2014), for instance, showed that the IRI  
80 2012 model entirely overestimates both monthly and seasonal VTEC values during phases of  
81 low solar activity. In addition, the model performance in estimating diurnal VTEC variations was  
82 found to be better during low solar activity phases than during high solar activity phases. In  
83 addition, the highest and the lowest values of the VTEC are observed in the equinoctial and the  
84 June solstice months, respectively during both the low and high solar activity phases. Abdu et al.  
85 (1996); Kakinami et al. (2012); Kumar et al. (2015) also attempted to describe the model's  
86 capacity to estimate the TEC using different versions of the model. **However, different findings**  
87 **show that the assessment of the improvement of the model performance from the relatively**  
88 **old to new versions for TEC estimation purpose in long lasting period is lacking over low**  
89 **latitude and equatorial regions, such as Ethiopia though the model has been steadily**  
90 **improved and arrived at the most recent version (IRI 2016). Hence, for a better**

91 **improvement of the IRI model in estimating the variation of TEC, its performance has to**  
92 **be continuously tested, especially over the equatorial and low latitude regions, where the**  
93 **dynamics of the ionosphere is very complex. In addition, there are few researches**  
94 **conducted to test the performance of IRI 2016 model over the region. The model includes**  
95 **some new features that are supposed to enhance its performance in estimating different**  
96 **ionospheric parameters. For instance, the two new model options for the F2-peak height**  
97 **hmF2 and a better representation of topside ion densities at very low and high solar**  
98 **activities enable the model in estimating *hmf2* directly and no longer through its**  
99 **relationship to the propagation factor  $M(3000)F2$ . As a result, the new model options make**  
100 **the IRI 2016 model estimate evening peaks that was not possible in the old versions.**

101 Thus, this study is mainly important to observe the TEC variation and the improvement of  
102 performance of the IRI model in estimating the TEC variation over low latitude African regions  
103 during the high solar activity phase (2013-2016) employing the GPS VTEC data inferred from  
104 different regions of Ethiopia. To observe the TEC variation and improvement of performance of  
105 the IRI model in estimating the TEC variation the latest versions (IRI 2007, IRI 2012 and IRI  
106 2016) with NeQuick option for the topside electron density during the solar maximum phase  
107 have been considered. The prediction performance of the model has been tested by comparing  
108 the modeled TEC values with the GPS-TEC values recorded in the receivers.

109

## 110 **2. Data description and analysis method**

111

### 112 *2.1. TEC from dual frequency GPS receiver*

113 As different studies (such as Ciruolo et al., 2007; Mannucci et al., 1998) show the GPS  
 114 measurements are used to estimate the TEC along a ray path between a GPS satellite and  
 115 receiver on the ground. These GPS measurements can be recorded using either single or dual  
 116 frequency GPS receivers. However, to eliminate ionospheric errors in the estimation of TEC dual  
 117 frequency receivers are better (Klobuchar, et al., 1996). Moreover, by computing the differential  
 118 phases of the code and carrier phase measurements, dual frequency GPS receivers can provide  
 119 integral information about the ionosphere and plasma sphere (Ciruolo et al., 2007; Nahavandchi  
 120 and Soltanpour, 2008). Hence, in this paper, the GPS-TEC data have been obtained from dual  
 121 frequency receiver using pseudo-range and carrier phase measurements. The TEC inferred from  
 122 the pseudo-range (P) measurement is given by:

$$123 \quad TEC_P = \frac{1}{40.3} \left[ \frac{f_1^2 f_2^2}{f_1^2 - f_2^2} \right] (P_2 - P_1). \quad (1)$$

124 Similarly, the TEC from carrier phase measurement ( $\Phi$ ) is given as

$$125 \quad TEC_\Phi = \frac{1}{40.3} \left[ \frac{f_1^2 f_2^2}{f_1^2 - f_2^2} \right] (\Phi_1 - \Phi_2), \quad (2)$$

126 where  $f_1$  and  $f_2$  can be related with the fundamental frequency,  $f_o = 10.23MHz$

$$127 \quad \begin{aligned} f_1 &= 154f_o = 1575.42MHz, \\ f_2 &= 120f_o = 1227.60MHz. \end{aligned} \quad (3)$$

128 As shown above, by cross correlating the  $f_1$  and  $f_2$  modulated carrier signals which are  
 129 generally assumed to travel along the same path through the ionosphere, the GPS receiver  
 130 obtains the time delay of the code and the carrier phase difference. The TEC obtained from code  
 131 pseudo-range measurements is free of ambiguity, but with relatively much noise. On the other

132 hand, the TEC obtained from carrier phase measurements has relatively less noise, but it is  
 133 ambiguous. Thus, linearly combining both code pseudo-range and carrier phase measurements  
 134 for the same satellite pass is believed to increase the accuracy of TEC (Ciraolo et al., 2007; Gao  
 135 and Liu, 2002; Klobuchar et al., 1996). This resultant absolute TEC is the GPS-derived STEC  
 136 along the signal from the satellite to the receiver on the ground. To better characterize the TEC  
 137 over a given receiver position and see the overall ionization of the Earth's ionosphere, the slant  
 138 TEC (STEC) must be converted into equivalent vertical TEC (VTEC) at the mean ionospheric  
 139 height,  $h_m=350$  km (Mannucci et al., 1998; Norsuzila et al., 2008, 2009). Hence, the relationship  
 140 between STEC and VTEC in terms of the zenith angle  $\chi'$  at the Ionospheric Piercing Point (IPP)  
 141 and the zenith angle  $\chi$  at the receiver position can be given by:

$$142 \quad VTEC = STEC(\cos \chi'), \quad (4)$$

143 where,

$$144 \quad \chi' = \arcsin\left[\frac{R_e}{R_e + h_m} \sin \chi\right]. \quad (5)$$

145 Substituting equation (5) into equation (4) and rearranging, we get

$$146 \quad VTEC = STEC \left\{ \cos \left[ \arcsin \left( \frac{R_e}{R_e + h_m} \sin \chi \right) \right] \right\}. \quad (6)$$

147 Here,  $R_e$  is the radius of the Earth in kilometers.

## 148 2.2. TEC from the International Reference Ionosphere (IRI) model

149 The International Reference Ionosphere (IRI) is an international empirical standard  
 150 model used for the specification of ionospheric parameters. The model provides average values  
 151  
 152

153 of electron density, electron content, electron and ion temperature, and ion composition as a  
154 function of height, location, local time, and sunspot number for magnetically quiet conditions  
155 (Bilitza, 2001; Bilitza et al., 2014; Bilitza et al., 2017). To enhance the capacity of the model,  
156 improvements have been made through the ingestion of all worldwide available data from  
157 ground-based as well as satellite observations. As a result, a new version of the model (IRI 2016)  
158 has been released in 2017 by incorporating some new input parameters that are supposed to  
159 increase its capacity. The IRI 2016 model includes two new model options for the F2-peak  
160 height  $hmF2$  and a better representation of topside ion densities at very low and high solar  
161 activities. The two new options are used in modeling  $hmf2$  directly and no longer through its  
162 relationship to the propagation factor  $M(3000)F2$ . Thus, the new model options enable the IRI  
163 2016 model to predict evening peaks that was not possible in the old versions. In addition, the  
164 improvement of the ion composition model in the topside ionosphere can lower the transition  
165 height from close to 1000 km down to almost 600 km in the new version of the model. A number  
166 of smaller changes have also been made concerning the use of solar indices and the speed-up of  
167 the computer program (Bilitza et al., 2017). For a given location, time and date, like the previous  
168 versions of the model, IRI-2016 model provides the monthly averages of ionospheric parameters  
169 (such as TEC) in the altitude range from about 50–2000 km (Bilitza et al., 2017;  
170 <http://IRImodel.org>). For more information, see the model web site  
171 (<http://omniweb.gsfc.nasa.gov/vitmo/iri-vitmo.html>) that was accessed for the period of 25-  
172 30/01/2018.

173

174 *2.3. Data sources and method of analysis*



175 The data required for both the experimental and model were obtained from Ethiopian **sites**  
176 shown in Figure 1 during the solar maximum (2013-2016) phase. Table 1 also shows the GPS  
177 receiver locations used for the study. The raw GPS data for the described station were obtained  
178 from the University NAVSTAR Consortium (UNAVCO web site, <http://www.unavco.org/>). The  
179 data gained from this web site have two forms: observation and navigation data in which both of  
180 them are zipped. To use the data for the desired purpose, the GG software (GPS-TEC calibrating  
181 software) was used to process the required data in five minutes interval and an elevation cut-off  
182  $10^\circ$ .

183 To get the required results, the corresponding modeled VTEC values were inferred from the  
184 latest versions of the model (IRI 2007, IRI 2012 and IRI 2016) that include some latest input  
185 parameters which are supposed to improve the capacity of the model in estimating ionospheric  
186 parameters. The online IRI versions of the model were obtained from  
187 <http://omniweb.gsfc.nasa.gov/vitmo.html>. To get the VTEC values, the year, date, month, location,  
188 the hour profile, the upper boundary altitude (2000 km), daily sunspot number and F10.7 cm  
189 flux, topside electron density options (NeQuick, IRI01, IRI2001), CCIR for F peak model, and  
190 ABT-2009 for bottomside thickness option were used as the input parameters,.

191 In order to observe the pattern of the hour-to-hour variability of VTEC, the mean monthly  
192 and seasonal hourly GPS TEC and the corresponding IRI TEC data have been used during the  
193 period of 2013-2016. To see the monthly and seasonal arithmetic mean VTEC variation and the  
194 model performance, the hour-to-hour measured and modeled VTEC values have been  
195 correspondingly added and averaged for the whole days in each month and season. The seasons  
196 could be classified as December solstice (November, December and January), March equinox  
197 (February, March and April), June solstice (May, June and July) and September equinox

198 (August, September and October). For a better understanding on the performance of the model,  
199 the absolute differences between the monthly and seasonal GPS VTEC and the corresponding  
200 IRI VTEC values have been determined. The differences have been calculated by subtracting the  
201 experimental VTEC values from the model. In order to clearly see the validation of the model,  
202 the absolute differences between the IRI VTEC and GPS VTEC in all the monthly and seasonal  
203 variations were determined. In addition, the percentage differences between the IRI VTEC and  
204 GPS VTEC for the arithmetic monthly and seasonal VTEC variations have also been determined.

### 205 **3. Results and discussion**

206 *3.1. Diurnal monthly and seasonal variation of VTEC and assessment of improvements in the*  
207 *performance of the IRI model*

208

209 **The results of the variations of the monthly and seasonal hourly VTEC are displayed in**  
210 **Figs 2-7. As observed in the figures, both the measured and modeled VTEC values start**  
211 **decreasing in the nighttime hours (00:00 UT or 03:00 LT) and become minimum after**  
212 **midnight hours (on average at 03:00 UT or 06:00 LT) and start increasing again to attain**  
213 **their peak values in the time interval of about 09:00-13:00 UT or 12:00-16:00 LT).**  
214 Moreover, in some hours, the modeled VTEC values (in all versions) are in a good agreement  
215 with the measured (GPS VTEC) values, especially in the nighttime hours (00:00-03:00 UT or  
216 03:00-06:00 LT). On the other hand, all versions of the model tend to underestimate the VTEC  
217 values during the daytime hours (09:00-13:00 UT or 12:00-16:00 LT). **Overestimations are also**  
218 **observed, especially in using IRI 2001 option for IRI 2012 model in 2013-2014 (see Figs. 4**  
219 **and 5) and using IRI 2016 model in 2016 (see Fig. 7). In the year 2013-2016, the highest**  
220 **underestimation (by about 30 TECU) and highest overestimation (by about 20 TECU) are**

221 **observed in the March equinox in 2015 (using IRI 2016 model) and June solstice in 2014**  
222 **(using IRI 2012 model with IRI 2001 option), respectively at about 12:00 UT (15:00 LT).**  
223 **However, IRI 2007 and IRI 2012 are generally better to capture the VTEC values as the**  
224 **solar activity decreases; while, IRI 2016 version is generally better when the solar activity**  
225 **increases (see Figs. 2-7). Moreover, the IRI 2012 version with NeQuick and IRI01-Corr**  
226 **gives hourly VTEC variation having closer hourly VTEC values (see Figs. 4 and 5). The**  
227 **mismodelings observed in both cases may be due to the difference in the model and experimental**  
228 **slab-thickness as noted by different findings (e.g. Nigussie et al., 2013; Rios et al., 2007). For**  
229 **instance, Rios et al. (2007) using the IRI 2001 model, showed that IRI predicted slab thickness is**  
230 **higher than the measured values except between (10:00-14:00 LT) which can attribute to VTEC**  
231 **fluctuations in similar trend. This is almost consistent with the result determined in this work.**  
232 **Using IRI 2007 model, Nigussie et al. (2013) also suggested similar possible reason for the**  
233 **discrepancy between the model and the experimental VTEC values. It could also be resulting**  
234 **from poor estimation of the hmF2 and foF2 from the coefficients, which in turn may result in**  
235 **poor estimation of VTEC by the IRI model (e.g. Chakraborty et al., 2014; Kumar et al, 2015).**  
236 **The underestimation of the IRI VTEC values by the GPS VTEC values may also attribute to the**  
237 **enhancement of the plasmaspheric electron content above 2000 km during the daytime hours**  
238 **(Coisson et al., 2008; Aggarwal, 2011; Venkatesh et al., 2011).**

239 **Moreover, the maximum peak of both the measured and modeled VTEC values are**  
240 **generally observed in the equinoctial months; while, the minimum peak values are observed in**  
241 **the June solstice months (see Fig. 2-7). For instance, over Arba Minch station (see Figs. 2 and 3),**  
242 **the highest and lowest peak measured monthly VTEC values of about 80 and 40 TECU are**  
243 **observed in March and July, respectively in 2015. Similarly, the highest and lowest peak**

244 modeled monthly VTEC values of about 55 and 41 TECU are observed in April and July,  
245 respectively in using IRI 2007 model with NeQuick option for the topside electron density. In  
246 addition, the highest and lowest peak measured seasonal VTEC values of are observed in the  
247 March equinox and June solstice, respectively in 2015. The highest and lowest peak modeled  
248 seasonal VTEC values of about 54 and 43 TECU are also observed in the March equinox and  
249 June solstice, respectively when using IRI 2007 model with NeQuick option for the topside  
250 electron density over Arba Minch station (see Fig. 6). In addition, in using IRI-2012 model with  
251 IRI2001 option for the topside electron density, the highest and lowest peak measured seasonal  
252 VTEC values of about 70 and 40 TECU are observed in the March equinox and June solstice,  
253 respectively over Ambo station in 2014. Similarly, the highest and lowest peak modeled seasonal  
254 VTEC values of about 74 and 60 TECU are observed in the March equinox and June solstice,  
255 respectively in 2014 when using the same version of the model (IRI 2012) with IRI2001 option  
256 (see Fig. 5). **The overall results show that, in the year 2013-2016, the highest peak measured**  
257 **VTEC values of about 80 TECU is observed in the March equinox in 2015.**

258 It is known that, in general, electron population in the ionosphere is mainly controlled by  
259 solar photoionization and recombination processes (Wu et al., 2004). Thus, for the equinoctial  
260 months, as the subsolar point is around the equator where the eastward electrojet associated  
261 electric field is often largest, it would be speculated that the peak photoelectron abundance and  
262 intense eastward electric field will be set up in the described region. On the contrary, for solstice  
263 months photoelectrons at the equator decrease as the subsolar point moves to higher latitudes.  
264 Moreover, the change of direction of neutral wind may account for the highest VTEC values in  
265 the equinoctial months and lowest values in the June solstice months. A meridional component  
266 of neutral wind blows from the summer to the winter hemisphere that is able to reduce the

267 ionization crest value during summer solstice as it blows in an opposite direction to the plasma  
268 diffusion process originating from the magnetic equator. Thus, in equinoxes meridional winds  
269 blowing from the equator to polar regions may attribute to a high ionization crest value. Hence, a  
270 seasonal effect on the crest should be expected with the crest maximum at the equinoxes and  
271 minimum in the summer season or June solstice (Bhuyan and Borah, 2007; Wu et al., 2004),  
272 which is consistent with the result of this work.

273

274 *3.2. Arithmetic mean of monthly and seasonal variations of VTEC and assessment of the*  
275 *improvements in the performance of the IRI model*

276 **The results of the arithmetic mean monthly and seasonal VTEC variations are given in**  
277 **Figures 8-11.** The results show that both the measured and the modeled arithmetic mean VTEC  
278 have generally the highest and lowest values in the equinoctial and June solstice months. For  
279 example, the highest and lowest measured arithmetic mean monthly VTEC values of about 38  
280 and 18 TECU are observed in April and July, respectively in 2014 over Ambo station (see the  
281 left top panel of Fig. 9). The seasonal measured arithmetic mean VTEC variation also shows the  
282 highest and lowest values of about 37 and 21 TECU in the March equinox and June solstice,  
283 respectively in 2014 (see the left bottom panel of Fig. 9). In addition, the highest and lowest  
284 seasonal measured VTEC values of about 36 and 23 TECU are observed in the March equinox  
285 and June solstice, respectively over Arba Minch station in 2015. The highest and lowest seasonal  
286 modeled arithmetic mean VTEC values of about 32 and 24 TECU are also observed in the March  
287 equinox and June solstice, respectively when using IRI 2007 version (see the left bottom panels  
288 of Fig. 10). On the other hand, the highest and lowest measured monthly VTEC values are  
289 observed in November and February, respectively in 2013. Similarly, the highest and lowest

290 measured seasonal VTEC values are observed in the December solstice and March equinox,  
291 respectively (see the left top and bottom panels of Fig. 8). But, the highest and lowest modeled  
292 arithmetic mean seasonal VTEC values are observed in the March equinox and June,  
293 respectively in 2013 when using IRI 2001 option for the topside electron density (see the left top  
294 panel of Fig. 8). **In the year 2013-2014, using the IRI 2012 model with IRI2001 option for the  
295 topside electron density shows the highest overestimation as compared to NeQuick and  
296 IRI01-Corr options. As shown in the Figures (see the right top and bottom panels of Figs. 8  
297 and 9), the highest monthly and seasonal overestimations are observed in July (by about  
298 130%) and the June solstice (by about 100%) in 2014. On the other hand, the IRI 2012  
299 version with NeQuick and IRI01-Corr option relatively gives VTEC having closer values  
300 (see Figs 8 and 9). Moreover, the IRI 2016 version shows overestimation of the VTEC as  
301 compared to others (IRI 2007 and IRI 2012), especially when the solar activity decreases.**  
302 For instance, the highest monthly and seasonal deviations of about 25% and 20% are observed  
303 between the modeled and corresponding measured values in September and the June solstice,  
304 respectively when IRI 2016 version is used (see the top and bottom right panels of Fig. 10).

305

### 306 *3.3 Storm Time VTEC variation and performance of the IRI model*

307 To see the VTEC variation and performance of the IRI model during storm time condition, the  
308 magnetic storm day (with Dst index maximum incursion of about -222nT) which occurred on  
309 March 17, 2015 as observed over Arba Minch station was considered (see Fig. 12). To better see  
310 the effect of the storm on the GPS VTEC and IRI VTEC, the pattern of the VTEC fluctuations in  
311 the initial phase (16/03/2015), main phase (17/03/2015) and in the recovery phase (18/03/2015)  
312 of the storm was considered. As shown in Fig. 13, the GPS-VTEC values show significant

313 fluctuation that indicates the occurrence of storm. On the other hand, the model VTEC values  
314 (IRI 2007, IRI 2012 and IRI 2016 VTEC) don't show any change when the storm model is "on"  
315 and "off" (see Figs.13a-13c and Figs.13d-13f). As shown in the figures, the mode VTEC values  
316 in all the three days follow almost similar pattern; they generally tend to underestimate the  
317 VTEC values (mostly after 08:00 UT or 11:00 LT) and remain smooth during the storm. This  
318 shows that the model does not respond to the effects resulting from storm. **The IRI 2016 VTEC**  
319 **values are also smaller than those of the IRI 2007 and IRI 2012 VTEC values in the initial,**  
320 **main and recovery phase of the storm.** In addition, enhancement of GPS TEC is observed as  
321 we proceed from the initial to the recovery phase of the storm. As shown in the figure, a peak  
322 VTEC value of about 65 TECU being observed in the initial phase increases to about 75 TECU  
323 in the recovery phase of the storm. This may be resulted from particle transport and the prompt  
324 penetration of high latitude electric fields (PPEFs) to lower latitude which travel equator ward  
325 with high velocities during the storm (Malik et al., 2010; Tsurutani et al., 2004; Sobral et al.,  
326 2001). **As the findings show, the dayside ionospheric storms resulting from PPEFs are**  
327 **characterized by transport of near-equatorial plasma to higher altitudes and latitudes,**  
328 **producing a giant plasma fountain. Hence, if the electric field penetrates into the dayside**  
329 **equatorial ionosphere, the plasma is convected toward higher altitudes, forming a giant**  
330 **plasma fountain. At these higher altitudes, the recombination rates are longer than for**  
331 **lower altitudes. On the other hand, solar photoionization at lower altitudes simultaneously**  
332 **continues to occur. This photoionization process will replace the uplifted plasma resulting**  
333 **in an overall increment of TEC.**

334

335 4. Conclusions

336           Because of the unique geometry of the geomagnetic field near the magnetic equator and low  
337 latitude regions (such as Ethiopia), the signal propagation system through the ionosphere is  
338 largely affected by the accumulation of electrons (TEC). Hence, in this study, the VTEC  
339 variation and the improvement of performance of the IRI model over the equatorial and low  
340 latitude regions has been studied employing the GPS and IRI techniques during the period of  
341 2013-2016. **The results reveal that the highest and lowest measured and modeled VTEC**  
342 **values are mostly observed in the equinoctial and June solstice months, respectively.**  
343 **However in 2013, the lowest and highest measured seasonal VTEC values are observed in**  
344 **the March equinox and December solstice, respectively. In the year 2013-2016, the**  
345 **maximum seasonal arithmetic mean measured VTEC values are observed in the March**  
346 **equinox except in 2013 in which the minimum and maximum being observed in the March**  
347 **equinox and December solstice, respectively.** In addition, though overestimation of the  
348 modeled VTEC has been observed on most of the hours, the model is generally good to estimate  
349 the diurnal hourly VTEC values mostly just after midnight hours (00:00-03:00 UT or 03:00-  
350 06:00 LT). It has also been shown that the model (IRI 2012) generally overestimates both the  
351 arithmetic mean of the monthly and seasonal hourly VTEC values, with the highest  
352 overestimation being observed in using IRI2001 option in 2013-2014. The overall results show  
353 that using NeQuick option for the topside electron density is generally better than other topside  
354 options for TEC estimation by IRI model. In general, the model does not show good  
355 improvements from version IRI 2007 to IRI 2016 in the TEC estimation over equatorial and low  
356 latitude regions. **However, the IRI 2007 and IRI 2012 versions are generally better to**  
357 **respond to the decrement of the VTEC values when the solar activity decreases; while IRI**  
358 **2016 version is generally better to capture the measured VTEC values when the solar**



359 **activity increases. Moreover**, all versions of the model do not respond to the effects resulting  
360 from storm. Hence, further improvements have to be made on the model for the betterment of its  
361 performance in estimating the VTEC over the equatorial and low latitude regions.

#### 362 **Author contribution**

363 All the required issues for the manuscript are prepared by the corresponding author, Yekoye

#### 364 **Competing interests**

365 The corresponding author declares that he has no conflict of interest.

#### 366 **Acknowledgements**

367

368 The data of daily sunspot number, GPS, Dst index and IRI model for this paper are freely  
369 available at: <http://www.sidc.be/sunspot-data/>,<http://facility.unavco.org/data/dai2/app/dai2..>,  
370 [http://wdc.kugi.kyoto-u.ac.jp/dst\\_final/201401/index.html](http://wdc.kugi.kyoto-u.ac.jp/dst_final/201401/index.html) and  
371 ([http://omniweb.gsfc.nasa.gov/vitmo/iri\\_vitmo.html](http://omniweb.gsfc.nasa.gov/vitmo/iri_vitmo.html)), respectively. Hence, the author is very  
372 grateful to UNAVCO, NOAA, World Data Center (Kyoto University) and NASA for donating  
373 their free GPS, daily sunspot number, Dst index and online IRI model data, respectively.

374

#### 375 **References**

376

- 377 Abdu, M.A., Batista, I.S.,Souza JR.(1996); An overview of IRI-observational data  
378 comparison in American (Brazilian) sector low latitude ionosphere. Adv Space  
379 Res 18(6):13-22.
- 380 Aggarwal, M. (2011); TEC variability near northern EIA crest and comparison with IRI model,  
381 Adv. Space Res., 48(7), 1221–1231, doi:10.1016/j. asr.2011.05.037

382 Asmare Y., Tsgaye, K., Melssew, N. (2014); Validation of IRI-2012 TEC model over  
383 Ethiopia during solar minimum (2009) and solar maximum (2013) phases. *Adv*  
384 *Space Res*, 1582-1594, <http://dx.doi.org/10.1016/j.asr.2014.02.017>.

385 Bhuyan, P.K., Borah,R.R. (2007); TEC derived from GPS net work in India and comparison  
386 with IRI. *Advances in Space Research: The Official Journal of the Committee on Space*  
387 *Research (COSPAR)* 39, 830-840.

388 Bilitza, D. (2001); International reference ionosphere 2000. *Radio Sci.* 36(2), 261-275.

389 Bilitza, D., D. Altadill, Y. Zhang, C. Mertens, V. Truhlik, P. Richards, L. McKinnell, and  
390 B. Bodo Reinisch, (2014); The International Reference Ionosphere 2012 – a model of  
391 international collaboration, *J. Space Weather Space Clim.*, 4, A07, DOI:  
392 10.1051/swsc/2014004

393 Bilitza1, D, D. Altadill, V. Truhlik, V. Shubin, I. Galkin, B. Reinisch, X. Huang (2017);  
394 International Reference Ionosphere 2016: from ionospheric climate to real-time weather  
395 predictions, *Space Weather*, DOI: 10.1002/2016SW001593.

396 Chakraborty,M., Kumar, S., Kumar, B., Guha, A.(2017); Latitudinal characteristics of GPS  
397 derived ionospheric TEC: a comparative study with IRI 2012 model, *Annals of*  
398 *Geophysics*, 57 (5), A0539; doi: 10.4401/ag-6438.

399 Ciraolo, L., F. Azpilicueta, C. Brunini, Meza, A. and S. M. Radicella (2007); Calibration errors  
400 on experimental slant total electron content (TEC) determined with GPS, *J., Geodesy*, 81,  
401 111–120

402 Coisson P., S. M. Radicella, L. Ciralo, R. Leitinger, and B. Nava (2008), Global validation of  
403 IRI TEC for high and medium solar activity conditions, *Adv. Space*  
404 *Res.*, 42, 770–775.

405 Ezquer, R.G., López, J.L., Scidá, L.A., Cabrera, M.A., Zolesi, B., Bianchi, C., Pezzopane M.,  
406 Zuccheretti, E., Mosert, M. (2014); Behaviour of ionospheric magnitudes of F2 region over  
407 Tucumán during a deep solar minimum and comparison with the IRI 2012 model  
408 predictions. *J. Atmos. Sol-Terr. Phys.* 107:89-98.

409 Gao, Y., Liu, Z.Z. (2002); Precise ionospheric modeling using regional GPS network data, *Journal*  
410 *of Global Positioning system*, vol. 1, No. 1:18-24.

411 Hansen, A., Blanch, J., T. Walter, T. (2000); Ionospheric correction analysis for WAAS quiet and  
412 stormy, in *Proceedings of the 13<sup>th</sup> International Technical Meeting of the Satellite Division*  
413 *of The Institute of Navigation ION GPS*, Salt Lake City, Utah, 19-22.

414 Hofmann-Wellenhof, B., Lichtenegger, H., Collins, J. (1992); *Global Positioning System Theory*  
415 *and Practice*. Springer-Verlag Wien, New York.

416 Hunsucker, R.D. and Hargreaves, R.D. (2003); *The high-latitude ionosphere and its effects on*  
417 *radio propagation*, Cambridge Univ. Press, UK.

418 Kakinami, Y., Liu, J.Y., Tsai, L.C. (2012); A comparison of a model using the FORMOSAT-  
419 3/COSMIC data with the IRI model. *Earth, Planets, Space*, 64:545-551.

420 Kelley, M.C. (2009); *The Earth's Ionosphere: Plasma Physics and Electrodynamics*,  
421 *Second Edition*. Elsevier Inc., New York.

422 Kumar, S., Tan, E., Murti. D. (2015); Impacts of solar activity on performance of the IRI-2012  
423 model predictions from low to mid latitudes. *Earth, Planets, Space*, 67:42.  
424 doi:10.1186/s40623-015-0205-3

425 Kumar, S. (2016); Performance of IRI-2012 model during a deep solar minimum and a  
426 maximum year over global equatorial regions, *J. Geophys. Res., Space Physics*, 121,  
427 doi:10.1002/2015JA022269.

428 Klobuchar, J.A., Parkinson, B.W., Spilker, J.J. (1996); Ionospheric effectson GPS, in: Global  
429 Positioning System: Theory and Applications, American Institute of Aeronautics and  
430 Astronautics, Washington, DC.

431 Lanyi, G.E. and Roth, T. (1988); A Comparison of Mapped and Measured Total Ionospheric  
432 Electron Content Using Global Positioning System and Beacon Satellite Observations.  
433 Radio Science, Vol. 23, No. 4, pp. 483-492.

434 Luhr, H., Xiong, C. (2010); IRI-2007 model overestimates electron density during the 23/24  
435 solar minimum, Geophysical Research Letters, Space Sciences, 37(23),  
436 <https://doi.org/10.1029/2010GL045430>  
437

438 Mannucci, A.J., Wilson, B.D., Yuan, D.N., Ho, C.H., Lindqwister, U.J.,Runge, T.F. (1998); A  
439 global mapping technique for GPS-derived ionospheric total electron content  
440 measurements. Radio Sci. 33, 565-582, <http://dx.doi.org/10.1029/97RS02707>.

441 Malik, Rakhee, Sarkar, Shivalika, Mukherjee, Shweta, Gwal, A.K (2010); Study of ionospheric  
442 variability during geomagnetic storms. J. Ind. Geophys. Union 14 (1), 47-56.

443 Misra, P., Enge, P. (2006); Global Positioning System: Signals, Measurements and Performance,  
444 2<sup>nd</sup> ed., Ganga-Jamuna Press, Lincoln, MA01773.

445 Nahavandchi, H., Soltanpour, A. (2008); Local ionospheric modeling of GPS code and carrier  
446 phase observation, vol. 40,309, pp.271-284.

447 Nigussie, M., Radicella, S.M., Damtie, B.,Nava,B., Yizengaw, E., Groves, K. (2013);  
448 Validation of the NeQuick 2 and IRI-2007 models in East-African equatorial region.  
449 J. Atmos. Sol-Terr. Phys., <http://dx.doi.org/10.1016/j.jastp.2013.04.016>.

450 Norsuzila, Y., Ismail, M., Abdullah M. (2008); Investigation of the GPS signals ionospheric  
451 correction: Ionospheric TEC prediction over equatorial region, IEEE International

452 Conference on Telecommunications and Malaysia International Conference on  
453 Communications (ICT-MICC 2007); Penang, Malaysia. 294-298, 14-17.

454 Norsuzila, Y., Mardina, A., Mohamod, I., Azami, Z. (2009); Model validation for Total  
455 electron content (TEC) at equatorial region, European Journal of scientific research vol.28,  
456 No.4, pp 642-648.

457 Olwendo, O.J., Baki, P., Mito, C., Doherty, P. (2012a); Characterization of ionospheric  
458 GPS total electron content (GPS TEC) in low latitude zone over the Kenyan region  
459 during a very low solar activity phase. *J. Atmos. Sol-Terr. Phys.*, 84-85:52-61.

460 Olwendo, O.J., Baki, P., Mito, C., Doherty, O. (2012b); Comparison of GPS TEC variations with  
461 IRI-2007 TEC prediction at equatorial latitudes during a low solar activity (2009-2011)  
462 phase over the Kenyan region. *J Adv Space Res.*  
463 <http://dx.doi.org/10.1016/j.asr.2012.08.001>.

464 Rios, V.H., Medina, C.F., Alvarez, P. (2007); Comparisons between IRI predictions and  
465 digisonde measurements at Tucuman. *J. Atmos. Sol. Terr.* 69, 569-577..

466 Sobral, J. H., M. A. Abdu, C. S. Yamashita, W. D. Gonzalez, A. C. de Gonzalez, I. S. Batista, C.  
467 J. Zamlutti, and B. T. Tsurutani (2001); Responses of the low-latitude ionosphere to very  
468 intense geomagnetic storms, *J. Atmos. Sol. Terr. Phys.*, 63, 965–974, doi:10.1016/S1364  
469 6826(00)00197-8.

470 Sethi, N., Dabas, R., Sarkar, S. (2011); Validation of IRI 2007 against TEC observations during  
471 low solar activity over Indian sector.

472 Tariku Y.A. (2015a); Patterns of GPS-TEC variation over low-latitude region (African sector)  
473 during the deep solar minimum (2008 to 2009) and solar maximum (2012 to 2013) phases.  
474 *Earth, Planets, Space* 67:35. doi:10.1186/s40623-015-0206-2.

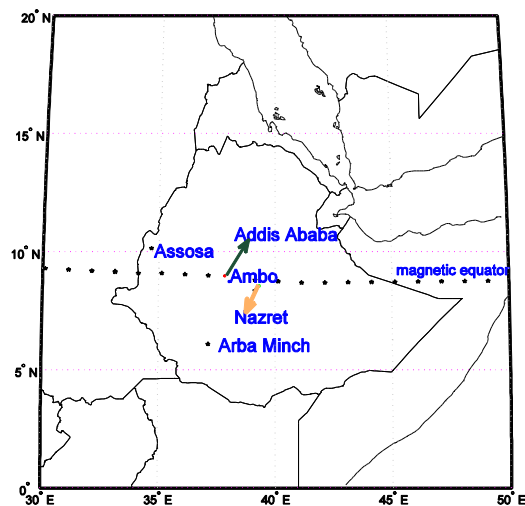
475 Tariku, Y.A. (2015b); TEC prediction performance of the IRI-2012 model over Ethiopia during  
476 the rising phase of solar cycle 24 (2009-2011), *Earth, Planets and Space* (2015) 67:140  
477 DOI 10.1186/s40623-015-0312-1.

478 Tsurutani, B., et al. (2004), Global dayside ionospheric uplift and enhancement associated with  
479 interplanetary electric fields, *J. Geophys. Res.*, 109, A08302, doi: 10.1029/2003JA010342.

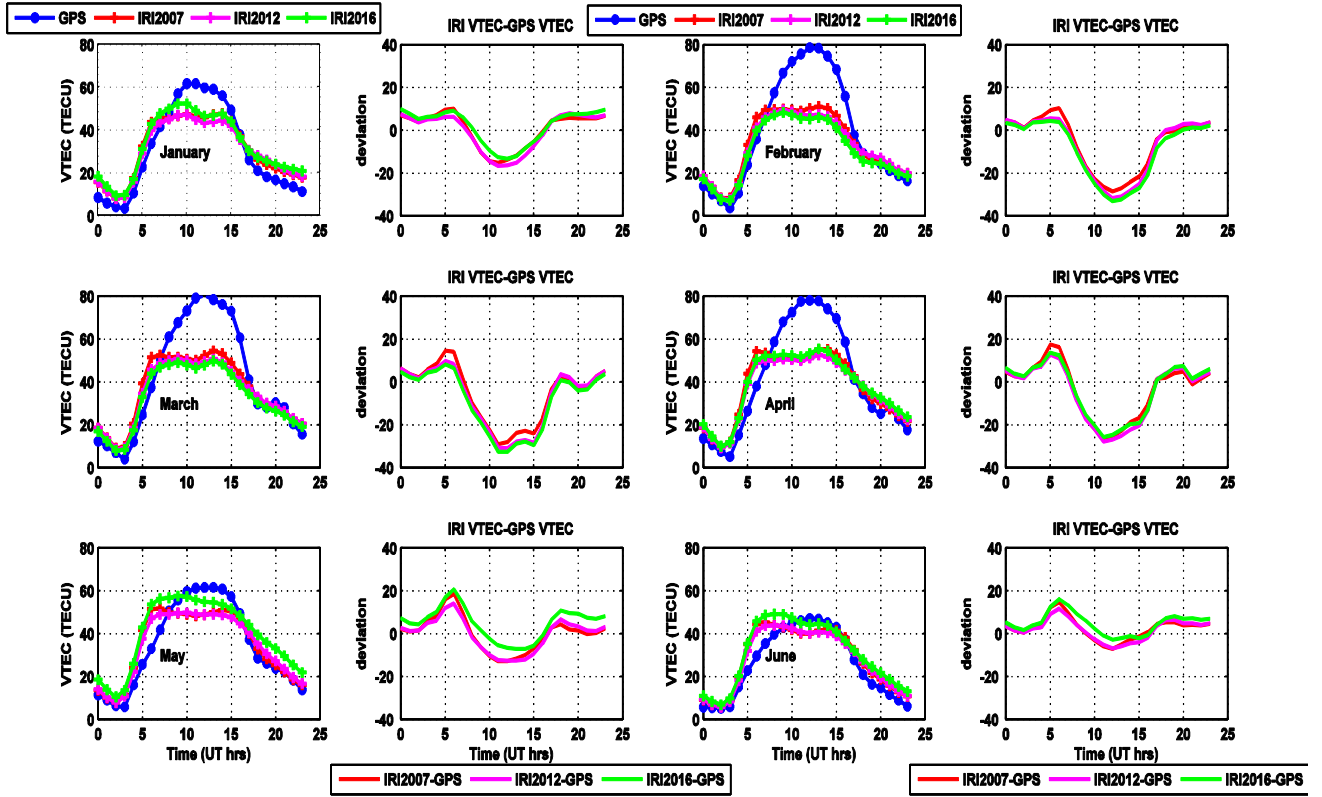
480 Venkatesh, K., P. V. S. Rama Rao, P. L. Saranya, D. S. V. V. D. Prasad, and K. Niranjan (2011),  
481 Vertical electron density and topside effective scale height (HT) variations over the Indian  
482 equatorial and low latitude stations, *Ann. Geophys.*, 29, 1861–1872, doi:10.5194/angeo-29-  
483 1861-2011.

484 Wu, C.C., Fry, C.D., Liu, J.Y., Liou, K., Tseng, C.L. (2004); Annual TEC variation in the  
485 equatorial anomaly region during the solar minimum: September, 1996-August 1997., *J.*  
486 *Atmos. Terr. Phys.*, 66:199-207.

487  
488 Figures



489  
490 Figure 1: Location of GPS receivers used for the study

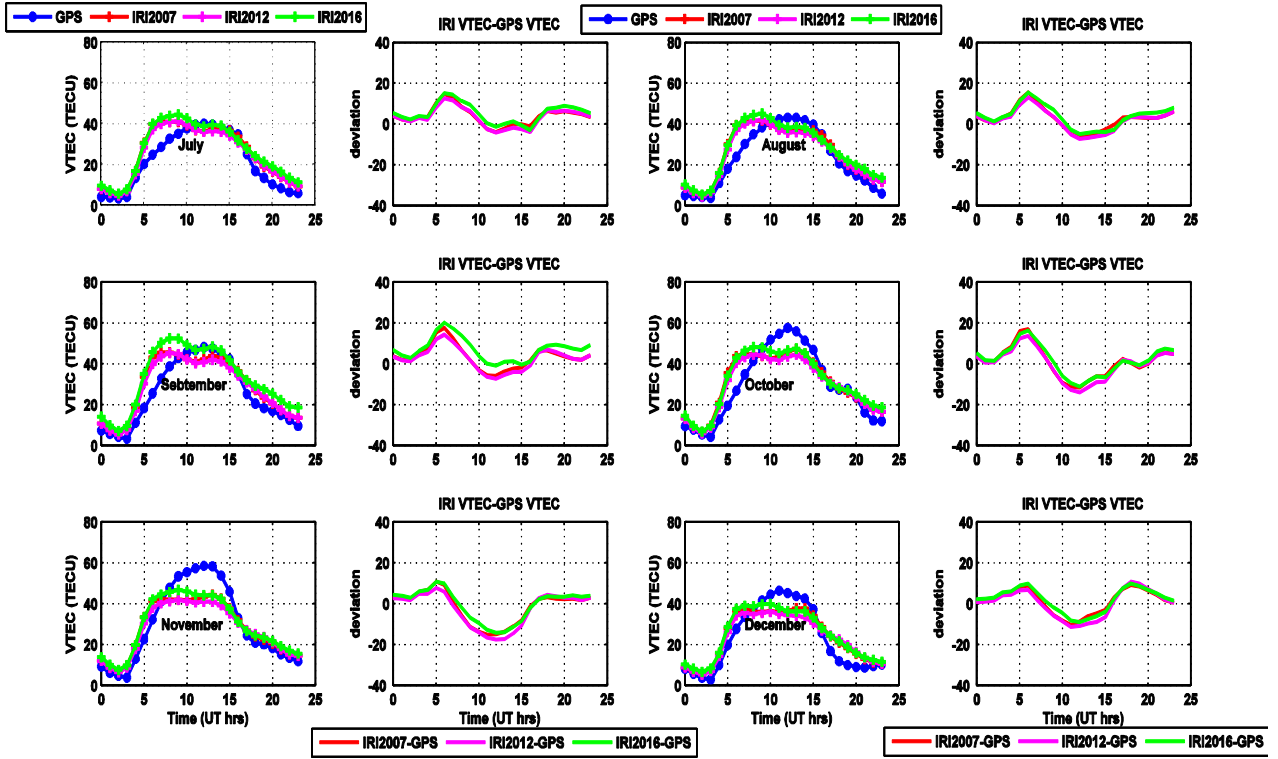


491

492 Figure 2: A graph to illustrate diurnal monthly VTEC variation and performance of the IRI

493 model over Arba Minch station during the period of January-June in 2015

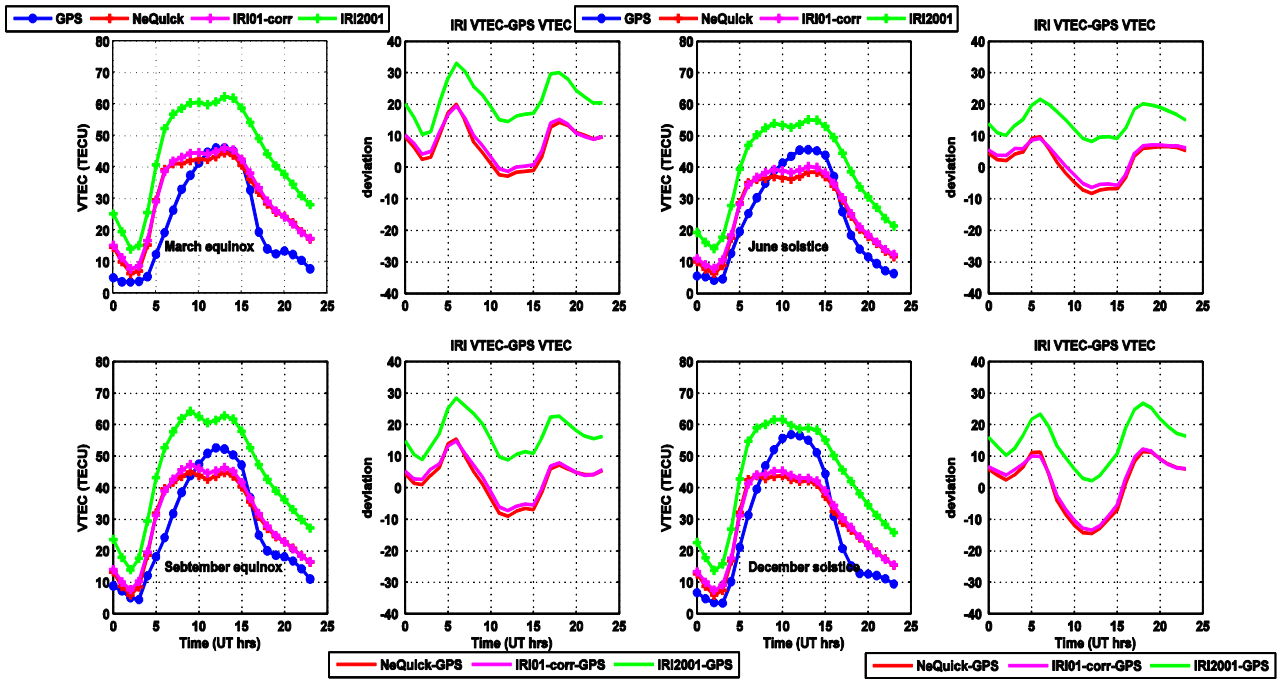
494



495

496 Figure 3: A graph to illustrate diurnal monthly VTEC variation and performance of the IRI

497 model over Arba Minch station during the period of July-December in 2015

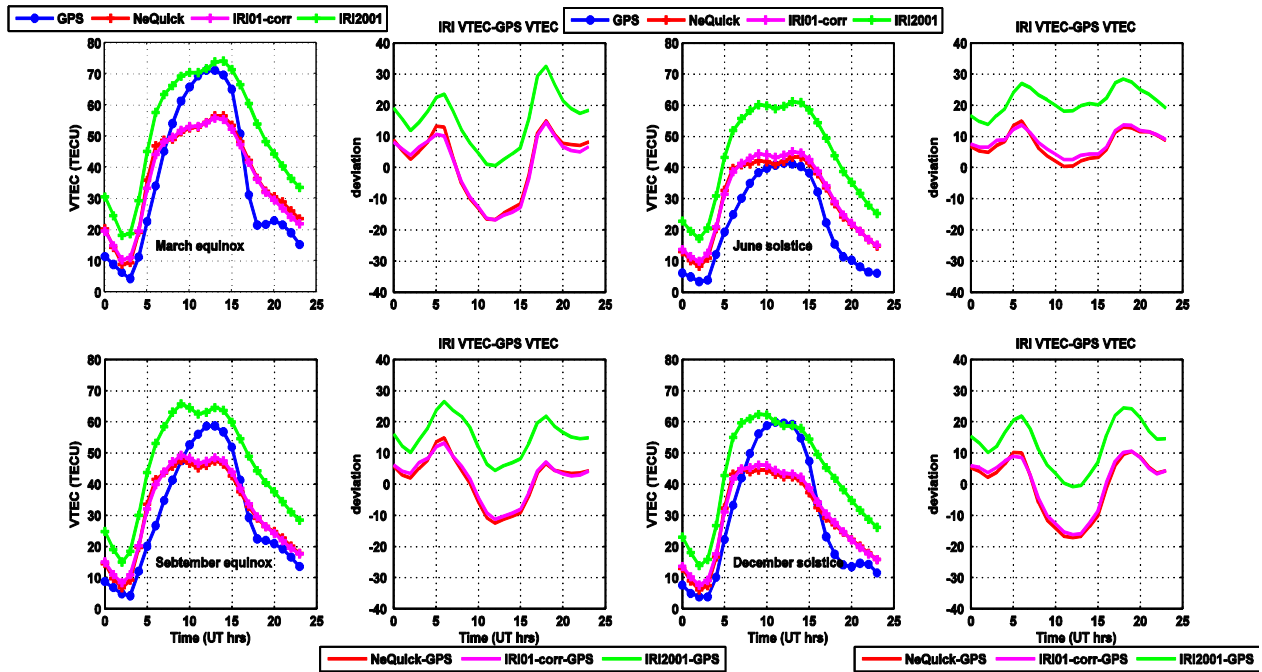


498

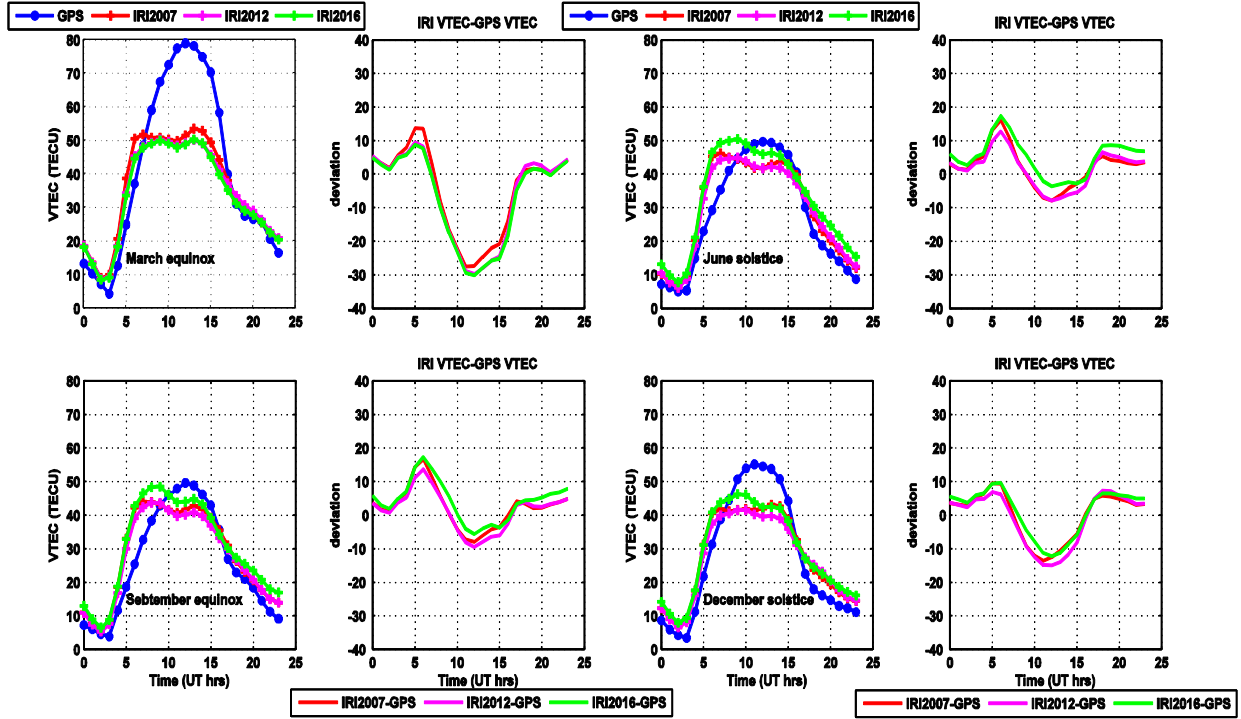
499



500 Figure 4: A graph to illustrate diurnal seasonal VTEC variation and performance of the IRI-2012  
 501 model over Ambo station during the period of 2013



502  
 503 Figure 5: A graph to illustrate diurnal seasonal VTEC variation and performance of the IRI-2012  
 504 model over Ambo station during the period of 2014

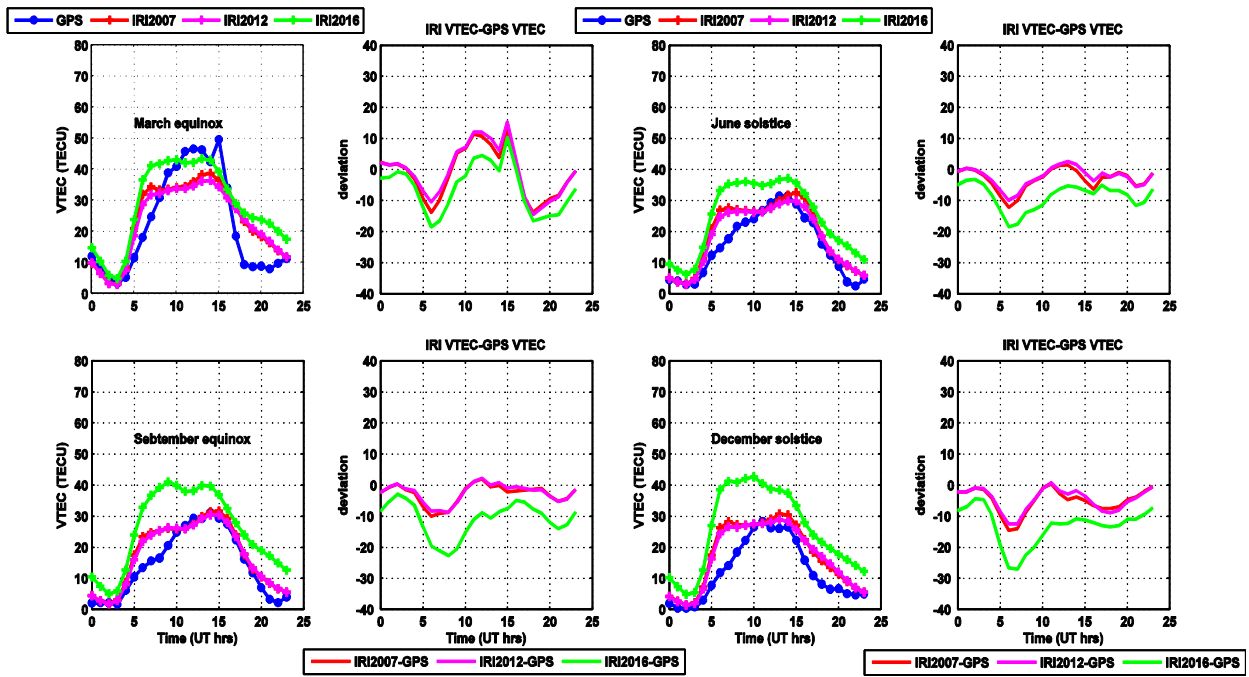


505

506

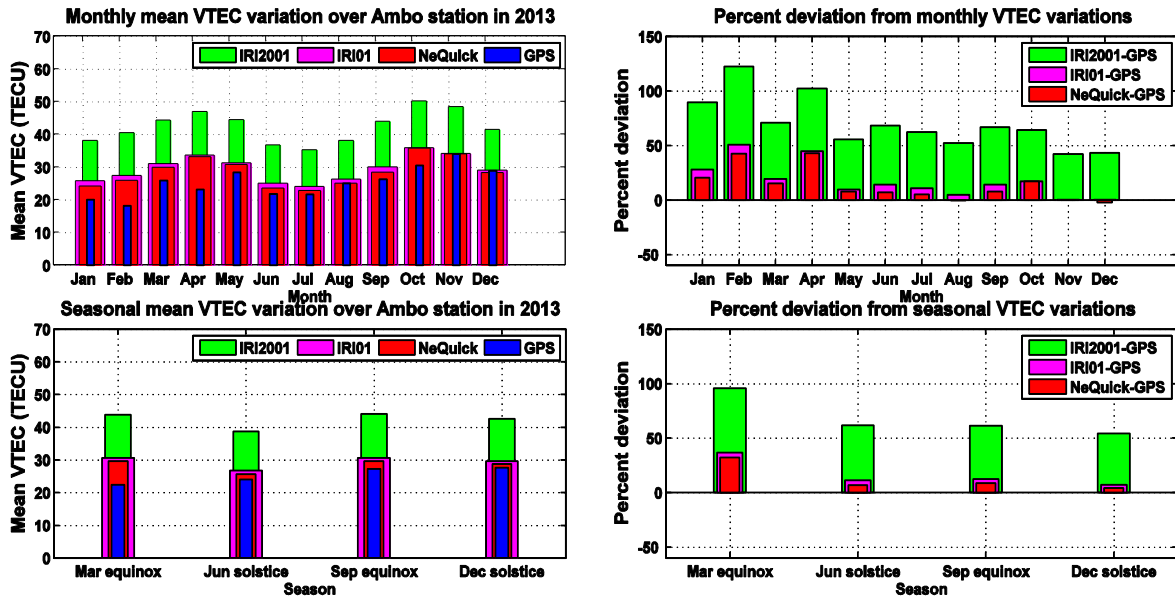
507 Figure 6: A graph to illustrate diurnal seasonal VTEC variation and performance of the IRI

508 model over Arba Minch station during the period of 2015

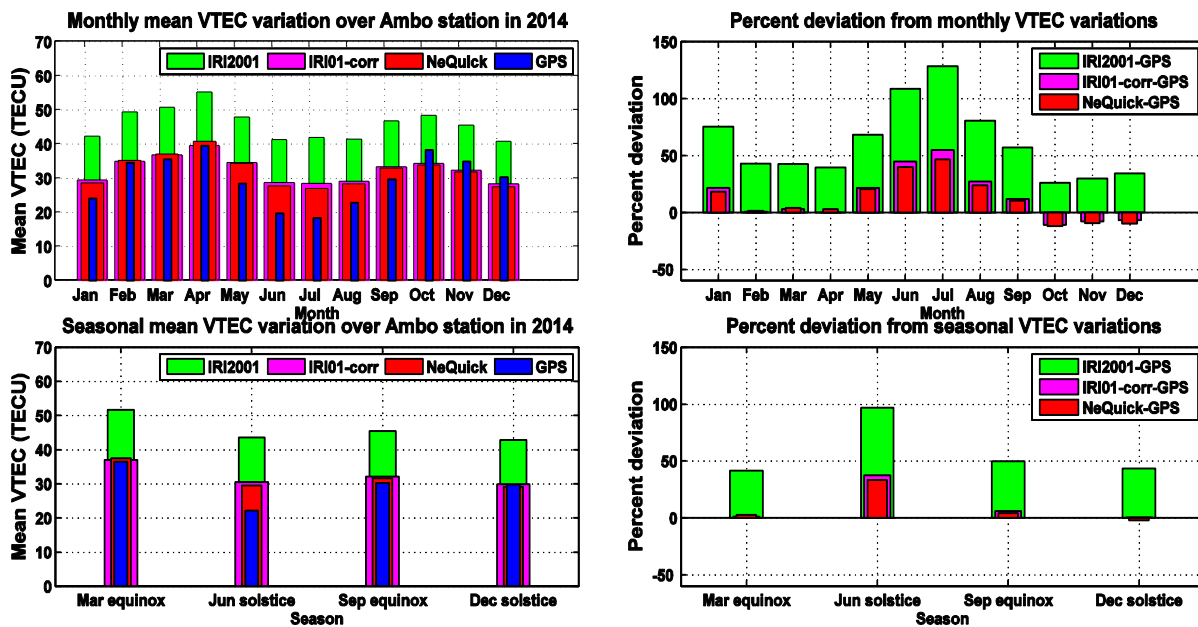


509

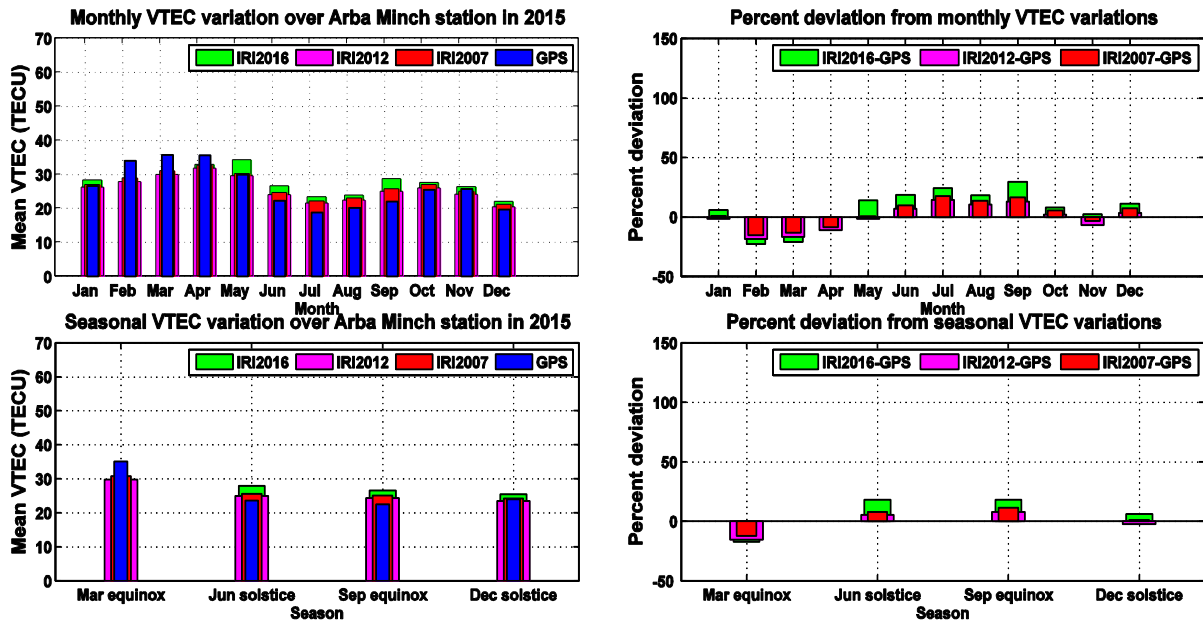
510 Figure 7: A graph to illustrate diurnal seasonal VTEC variation and performance of the IRI  
 511 model over Asosa station during the period of 2016



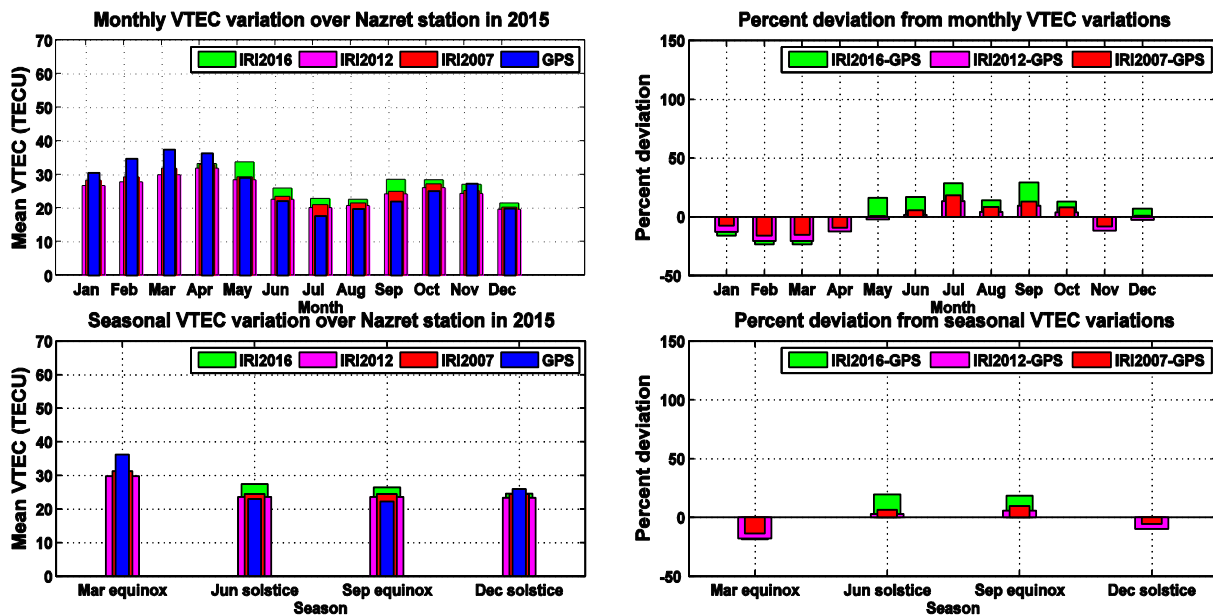
512  
 513 Figure 8: A graph to illustrate the arithmetic mean monthly and seasonal VTEC variation and  
 514 performance of the IRI-2012 model over Ambo station during the period of 2013



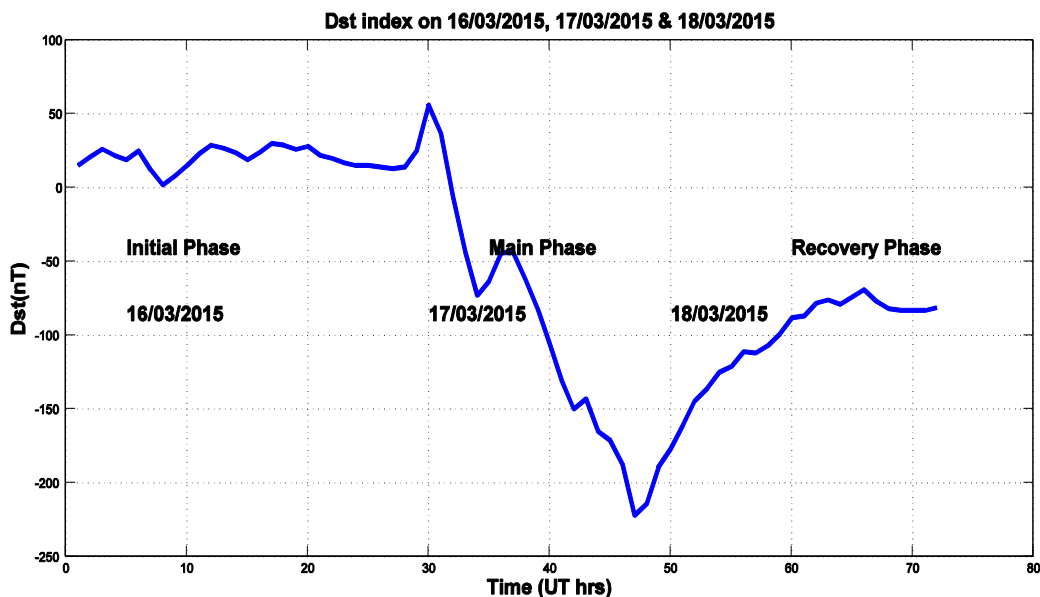
516 Figure 9: A graph to illustrate the arithmetic mean monthly and seasonal VTEC variation and  
 517 performance of the IRI-2012 model over Ambo station during the period of 2014



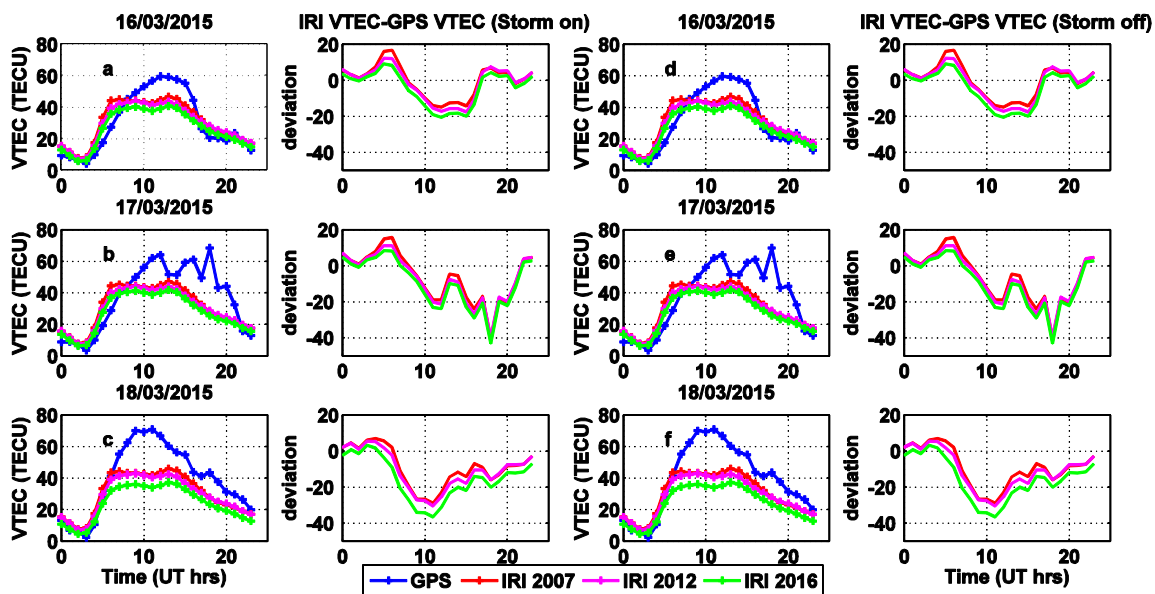
518  
 519  
 520 Figure 10: A graph to illustrate the arithmetic mean monthly and seasonal VTEC variation and  
 521 performance of the IRI model over Arba Minch station during the period of 2015



523 Figure 11: A graph to illustrate the arithmetic mean monthly and seasonal VTEC variation and  
 524 performance of the IRI model over Nazret station during the period of 2015



525  
 526  
 527 Figure 12: Dst index on 16/03/2015, 17/03/2015, and 18/03/2015 as observed over Arba Minch  
 528 station during the period of 2015 (data source for Dst index: World Data Center, Kyoto  
 529 University).



530

531 Figure 13: A graph to show the variation of the VTEC and the response of IRI model on storm  
 532 time condition which occurred on March 17/2015 as observed over Arba Minch station. Figures  
 533 14a–14c and Figures 14d–14f show patterns of the modeled and measured VTEC values when  
 534 the storm option is “on” and “off,” respectively.

<b>Station</b>	<b>code</b>	<b>Geographic coordinates Lat. (N), Long. (E)</b>	<b>Geomagnetic coordinates Lat. (N), Long. (E)</b>	<b>Dip angle</b>
<b>Asosa</b>	asos	(10.05,34.55)	(0.56,106.38)	3.2
<b>Ambo</b>	aboo	(8.97,37.86)	(0.07,109.80)	1.2
<b>Nazret</b>	nazr	(8.57,39.29)	(-0.08,111.27)	1.19
<b>Arba Minch</b>	armi	(6.06,37.56)	(-3.08,109.57)	-5.7

535  
 536

537 Table 1: Coordinates of GPS receivers used for the study

538